Electronic Journal of Structural Engineering

Original Article

Cite this: DOI:10.56748/ejse.24548

Received Date:09 November 2023
Accepted Date: 06 July 2024

1443-9255
https://ejsei.com/ejse

Numerical Modeling of Steel Fiber Reinforced Recycled Concrete Filled Steel Tube Column Under Cyclic Loading

Mohamed A. Sakr[a], Ayman A. Seleemah[a], Omnia F. Kharoob[a], Mostafa M. Aboelnour[a]*
[a] Dept. of Structural Engineering, Tanta University, Tanta, Egypt.
*Corresponding author: Mostafa.Aboelnor@f-eng.tanta.edu.eg

Abstract

A finite element model (FEM) was created with the aim of analyzing the behavior of steel fiber reinforced recycled concrete (SFRRC)-filled steel tube columns under combined cyclic loading and monotonic axial load. The FEM by ABAQUS considered the effect of steel tube confinement on the inner concrete behavior under cyclic loading. The numerical model was described in detail, with a focus on modeling the materials involved (normal concrete, SFRRC, and steel) under cyclic loading. A constitutive concrete model - with and without considering confinement - was based on utilizing a concrete damaged plasticity (CDP) model. The steel tube - concrete core interface was modeled by a surface-to-surface contact. A stress-strain constitutive concrete model, confined by circular steel tubes, was implemented, and validated using experimental results from the literature. The developed FEM considered various parameters: steel tube thickness, volume ratios of steel fibers, besides strengths of both concrete core and the steel tube. The FEM results showed great agreement with the experimental results under cyclic loading. The results indicated that the concrete confining pressure must be considered in CDP model. A good correlation between numerical and experimental findings was obvious, including failure modes, and hysteretic curves of load-displacement.

Keywords

FE modeling, Steel fiber reinforced recycled concrete, Concrete-filled steel tube (CFST) Columns, Cyclic loading

1. Introduction

The recent popularity of concrete-filled steel tubular (CFST) columns in engineering construction is the result of their excellent behaviors concerning ductility, strength, seismic performance, fire resistance, lateral stiffness, and energy dissipation capacity. A CFST column is best featured by components' decline in cross-section, a rise in the availability of structures' space and a fall in the structure self-weight (Y. Chang, Chen, Xiao, Rong, & Peng, 2021; Han, Li, & Bjorhovde, 2014; Ibañez, Hernández-Figueirido, & Piquer, 2021; X. Liu, Liu, Yang, Cheng, & Lanning, 2020; Nguyen, Thai, Ngo, Uy, & Li, 2021; Qu, Xie, Sun, Liu, & Wang, 2023; Tu, Shi, Liu, Wang, & Ban, 2021). Concrete combined with steel tube in CFST columns has resulted in their extensive usage as frame columns in high-rise buildings, with the core concrete confined by the steel tube, enhancing both ductility and strength with prevention of concrete spalling (Di, Han, et al., 2022; J. Liu, Zhou, & Zhang, 2008; Lue, Liu, & Yen, 2007; Probst, Kang, Ramseyer, & Kim, 2010; Yıldızel et al., 2023). Consequently, core concrete causes protection, and delays local buckling of the steel tube (X. Chang, Fu, Zhao, & Zhang, 2013; Di, Fan, et al., 2022; Fayed, Badr el-din, Basha, & Mansour, 2022; Lai & Ho, 2015; Madenci, Fayed, Mansour, & Özkılıç, 2022; A. Zhu, Zhang, Zhu, Zhu, & Lu, 2017). No further reinforcement is required since the steel tube plays the role of both concrete lateral and longitudinal reinforcement. Practically, steel tubes function as permanent formwork in the construction of multistory buildings, aiming at efficient reduction of construction challenges and duration (Chen, Wang, Xie, & Jin, 2016).

The tubes' diameter- to - thickness ratios (D/t) influence the concrete confinement. As indicated by (Han, Huang, Tao, & Zhao, 2006), the CFST ultimate strength is much greater compared to individual strength summation of both the reinforced concrete column and the steel tube. This can be illustrated as follows: "1(steel tube) + 1(concrete core) > 2 (the two materials simple summation)". Therefore, using CFST leads to efficiency in bridge piers and other columns.

The few recent decades have witnessed conducting several quasistatic cyclic loading tests in investigation of the CFST columns' seismic behavior (Emad et al., 2022; Fam, Qie, & Rizkalla, 2004; Ge & Usami, 1996; Hajjar & Gourley, 1997; Morishita, 1982; Tam, Minkeng, Lau, Mansour, & Wu, 2023; H. Zhu, Zhang, & Liu, 2021). However, the widespread of using normal concrete (NC) in the construction of bridges as well as other buildings around the world needs further addressing due to the remarkably contrary effluence as a result of its brittle property affecting the components of the structures during seismic responses. Concerning material qualities and modifying the brittle nature of NC, researchers' efforts have involved steel tube filled with concrete. This traditional technique modifies the NC brittle properties. Latest studies (Amin, Agwa, Mashaan, Mahmood, & Abd-Elrahman, 2023; Gopal & Manoharan, 2006; Jaf et al., 2023; Y. Lu, N. Li, S. Li, & H. Liang, 2015; Osama & Sakr, 2023; Saad, Sakr, Khalifa, & Darwish, 2023; Tokgoz & Dundar, 2010) point out that core concrete properties could considerably affect the ductility of CFST columns, achieving a higher ductility by using steel fiber reinforced concrete (SFRC) instead of NC. Additionally, extra investigations demonstrate that the insertion of steel fibers into the matrix might provide a similar result on the SFRCFST columns (Aksoylu, Özkılıç, Hadzima-Nyarko, Işık, & Arslan, 2022; Choi, Jung, & Choi, 2013; ELWakkad, Heiza, & Mansour, 2023; Fayed, Madenci, Özkiliç, & Tawfik, 2024; Y.-y. Lu, N. Li, S. Li, & H.-j. Liang, 2015; Madenci et al., 2022; Xu, Wu, Liu, & Shao, 2019; Zeybek et al., 2022).

Recently, there have been large quantities of concrete waste resulting from the demolition of old buildings. Therefore, it is important to use recycled concrete (RC). Recycled concrete is manufactured from recycled coarse aggregate (RCA) that we obtain from crushing and processing concrete waste (Fayed, Madenci, Bahrami, Özkiliç, & Mansour, 2023; Fayed, Madenci, Özkiliç, & Mansour, 2023; Mansour, Li, Wang, & Badawi, 2024; Xiao & Xiao, 2018; Yildizel, Özkılıç, & Yavuz, 2024). (RC) can reduce environmental pollution and it can help preserve natural resources. Moreover, adding steel fibers to recycled concrete can improve performance in compressive and tensile, which is called steel fiber reinforced recycled concrete (SFRRC) (Fantilli, Vallini, & Chiaia, 2011; Song & Hwang, 2004; Yu, Lin, Geng, Wei, & Jia, 2013) to develop the application of RAC. One of the innovative composite columns involves filling (SFRRC) into the steel column tube. (Zhao, Huang, Liu, Wang, & Lu, 2022) identifies this as steel fiber reinforced recycled concrete filled steel tube (SFRRCFST) column. This composite element SFRRCFST column can compensate for the side effects of recycled concrete by filling the steel tube with it. The tube can confine RAC and protect it. Which produces triaxial-compressive state, which leads to an increase in compressive strength, deformation ability, and durability. At the same time, the concrete prevents the local buckling of the steel tube (ACI, 2014; Z. Liu, Lu, Li, & Liao, 2019, 2021; Z. Liu, Lu, Li, Zong, & Yi, 2020; Zhao et al., 2022). It was important to study the possibility of using SFRRCFST column in seismic areas. (Zhao et al., 2022) study the seismic performance of SFRRCFST columns, 14 circular specimens with different parameters, volume fractions (Vf) of steel fiber, axial compression ratios (n), steel tube thickness (t), and concrete strengths were tested to failure under constant axial and lateral cyclic loads. All specimens showed the same type of failure, and it was compression bending failure. The deterioration of the stiffness, the deterioration of the strength, the ability to dissipate energy, and the hysteresis curve were all obtained under the influence of various

parameters. Regarding the results obtained by the research, it is that adding steel fibers to recycled concrete improves its behavior in general in compression and tension. It is clear that increasing the volume of steel fibers led to an improvement in the lateral load capacity, as well as ductility and energy dissipation. It is also important that increasing the thickness of the steel tube led to a very clear improvement in the overall seismic behavior. Moreover, the seismic performance became lower when the axial pressure ratio increased, and this was evident in the amount of deformation and ductility.

To the authors' knowledge, the majority of recently performed studies have experimentally focused on studying the behaviors of NCFST and SFRRCFST columns under combined cyclic loading and monotonic column axial load with only a few numerical analyses. Conducting experimental studies on these columns can be expensive, which is why the authors of this paper aim to bridge this gap by developing a reliable numerical model. The objective is to create a simulation that accurately replicates the behavior of NCFST and SFRRCFST columns under lateral cyclic loading, ensuring its validity and accuracy with available experimental tests. Presentation and description of the numerical model is initially done in detail, followed by validation of numerical results through comparison with the specimens confirmed experimentally by (Zhao et al., 2022). The developed FEM takes into account key parameters of considerable effect on the (CFST) columns behavior. These parameters include steel tube thickness (t), steel fibers volume ratios (Vf), besides strengths of both steel tube (fy) and concrete (fc).

2. Finite element models' description

Utilizing ABAQUS Version 6.2 (D. S. Simulia, 2013), numerical modeling of NCFST and SFRRCFST columns with circular cross-sections investigated by (Zhao et al., 2022) under mixed cyclic lateral loading and monotonic column axial load are discussed in this part. A detailed 3-dimensional (3D) model is implemented to provide the anticipated behavior with a detailed description of the constitutive models used throughout the procedures.

2.1 Properties of materials and constitutive models

Unconfined concrete

For unconfined concrete the "Concrete damage plasticity model" (CDP) was utilized to simulate the nonlinear behavior of concrete (Sakr, El-Khoriby, Seleemah, Aboelnour, & Osama, 2021). This damaged plasticity model is

usually recommended to have a general capacity to analyze quasi-brittle

materials under monotonic, cyclic, and/or dynamic loading (A. U. M. Simulia, 2007). Compressive crushing and tensile cracking are the two major failure mechanisms in the CDP model (A. U. M. Simulia, 2007), the compression stress–strain response suggested by Saenz(Desayi & Krishnan, 1964) was used as shown in Fig.1. To draw the tension stress–strain response, the elastic modulus, and tensile strength, f_{ct} parameters are needed(ACI Committee, 2008).

Confined concrete

When the concrete is under triaxial stress, compressive strength in a uniaxial direction becomes enhanced, besides a rise in the associated strain. Moreover, the hoop stress variable of the circular CFST column's stress causes the internal concrete to be confined with stress in the axial direction.

The elastic behavior of concrete reaches a stress up to 0.4 f'_c, according to EN 1992-1-1 (Européen, 2004), hereafter, the concrete's plasticity curve in compression begins. A corresponding uniaxial stress-strain curve for the confined and unconfined concrete is shown in Fig. 1. At this point, f '$_c$ (0.8 f_c) denotes the unconfined concrete strength, ε'_c denotes the corresponding unconfined strain, assumed to be 0.003 by the ACI Specification (ACI, 2014), f'_{cc} denotes the strength of confined concrete, and ε'_{cc} denotes the corresponding confined strain. According to the following relationships suggested by (Mander, Priestley, & Park, 1988) and determining the values of f'_{cc} and ε'_{cc}:

$$f'_{cc} = f'_c + k_1 fl \quad (1)$$

$$\varepsilon'_{cc} = \varepsilon'_c \left[1 + k_2 \frac{f_l}{f'_c}\right] \quad (2)$$

At this point, fl stands for the steel tube confining pressure. (Hu, Huang, Wu, & Wu, 2003) proposed a formula that can be used to determine the value of fl:

$$f_l/f_y = \begin{cases} 0.043646 - 0.000832(D/t) & (21.7 \le D/t \le 47) \\ 0.006241 - 0.0000357(D/t) & (47 \le D/t \le 150) \end{cases} \quad (3)$$

Here f_y refers to the steel tube yield strength. (Richart, Brandtzæg, & Brown, 1928) provided values of the parameters k1 and k2 as 4.1 and 20.5, respectively, while (Mander et al., 1988) made a proposal of the widely approved constitutive relationship in the following Eqs. (4,5 and 6), is adopted when $\varepsilon_c \le \varepsilon'_{cc}$.

$$\sigma_c = \frac{f'_{cc}\,\lambda(\varepsilon_c/\varepsilon'_{cc})}{\lambda - 1 + (\varepsilon_c/\varepsilon'_{cc})^{\lambda}} \quad (4)$$

$$\lambda = \frac{E_c}{E_c - (f'_{cc}/\varepsilon'_{cc})} \quad (5)$$

$$E_c = 4700\sqrt{\gamma c\, f'_c}\ \text{(MPa)} \quad (6)$$

The concrete strength is determined through implementation of the factor γ_c, which was expressed by (Liang, 2009) as follows:

$$\gamma_c = 1.85\ D_c^{-0.135} \quad (0.85 \le \gamma_c \le 1.0) \quad (7)$$

as Dc = D – 2t denotes the filled concrete's diameter, whereas D refers to the tube's diameter and t for its thickness.

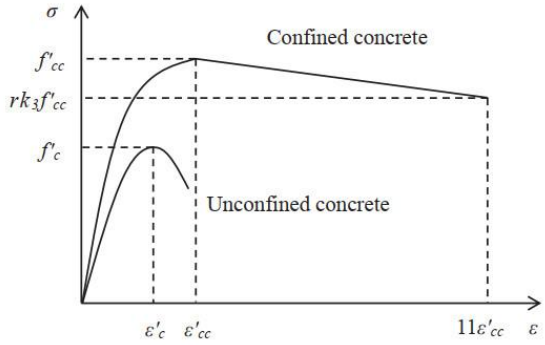

Fig. 1 Constitutive relationship of confined concrete (Mander et al., 1988)

The relationship of stress-strain is presumed to be linear when $\varepsilon_c > \varepsilon'_{cc}$. The descending line can be determined by $f_c = rk_3 f'_{cc}$ while its ending point $\varepsilon_c = 11\,\varepsilon'_{cc}$. The corresponding values of r to concrete cube strengths of 30 MPa and 100 MPa are set to 1.0, and 0.5, respectively. The linear interpolation approach can be used to determine the value of r in general. Eq. (8) from (Hu et al., 2003) determines the parameter k3 as follows:

$$k_3 = \begin{cases} 1 & (21.7 \le \frac{D}{t} \le 40) \\ 0.0000339(D/t)^2 - 0.010085(D/t) + 1.3491 & (40 \le D/t \le 150) \end{cases} \quad (8)$$

The Concrete damaged plasticity CDP model was utilized to model the unconfined concrete and confined concrete material. The following are the plasticity parameters as specified by (Tao, Wang, & Yu, 2013): (e) was the flow potential eccentricity taken as 0.1, the viscosity parameter was 0, (Kc) was The ratio of the 2nd stress invariant on the compressive meridian to the tensile meridian taken as 0.7157, (ψ) was the dilation angle taken as 29.39° (calibrated) and (B f_{b0}/f'_c) was the compressive strength beneath biaxial loading with regard to the compressive strength under uniaxial loading taken as 1.1174.

The CDP model necessitates the definition of the aforementioned parameters in addition to the compressive and tensile stress-strain curves of the concrete via presenting data in tables (pairs of stresses-σ, strains-ε). The proper commands of ABAQUS (D. S. Simulia, 2013) (Concrete Compression Hardening and Concrete Tension Stiffening) were used to accomplish this. The model proposed by (Hognestad, 1951) and (Kent & Park, 1971) was based on the idea that concrete's uniaxial compressive and tensile behavior was affected by damaged plasticity, as seen in Fig. 2.

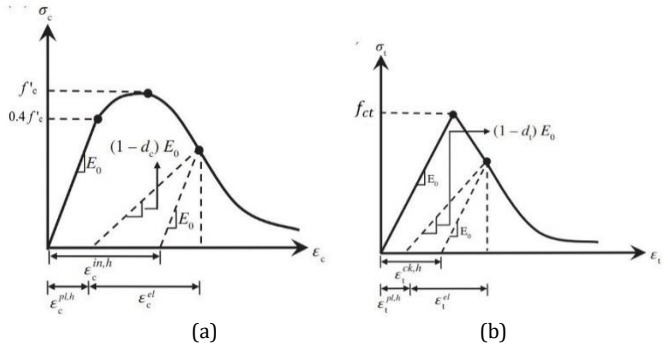

Fig. 2 Concrete response of a uniaxial loading condition (a) Compression, (b)Tension. (Hognestad, 1951) and (Kent & Park, 1971)

In addition to defining the concrete compressive hardening, i.e. the compressive stress-strain curve, the usage of the concrete compression damage command is suggested (D. S. Simulia, 2013) to account for the cyclical behavior of concrete. By using the damage parameter in compression (dc), which ranges from 0 (no damage) to 1 (complete

damage), this is utilized to define, for each value of strain, the damage state of the concrete stiffness (Sakr, Saad, & El-korany, 2022). Compression damage (dc) is so related with the inelastic hardening strain in compression $\varepsilon_c^{in,h}$, controlling the slope of the unloading curve since an increase in $\varepsilon_c^{in,h}$ leads to an increase in dc, which can be defined as:

$$d_c = 1 - \frac{\sigma_c}{f'_c} \quad (9)$$

In brittle materials (like concrete and similar materials), as a result of damage, when plastic strains grow, the tangent of the curve decreases compared to the initial tangent (modulus of elasticity, E0), as seen in Fig. 2a. At the maximum value of compressive stress, the damage parameter (dc) is zero. Thereafter, it starts to change and keeps changing until it reaches 0.8 with regard to 20% of the residual strength under great strains. Despite the existence of several constitutive models for concrete in the tension phase, no obvious changes in results are found due to the brittle behavior of concrete. As a ratio of compressive strength (f'_c), the highest value of tension phase is chosen in accordance with the following equation for constitutive models:

$$f_{ct} = 0.33\sqrt{f'_c} \quad (10)$$

as f'_c is compressive cylinder strength

Fig. 2b shows that the increase in tension damage is so related to the increase in the hardening cracking strain, $\varepsilon_{ck}{}^{t}$, which is to be expressed through the following equation:

$$d_t = 1 - \frac{\sigma_t}{f_{ct}} \quad (11)$$

Steel tube

In this investigation, steel material was modeled using the Chaboche model (Chaboche, 1986, 1989), an elastic-plastic stress-strain law with combined isotropic/kinematic hardening. The experimental values of Young's modulus (E_s) and Poisson's ratio (v_s) were utilized to determine the elastic properties.

The Chaboche model can be represented in ABAQUS as a plastic constitutive model with defining its parameters (σ_0, Q_∞, b, $C_1$and γ_1), where at zero plastic strain σ0 is the yield stress; the isotropic hardening parameters are Q_∞ and b; the kinematic hardening parameters are C_1 and γ_1.

The part of isotropic hardening in the steel constitutive law reads (D. S. Simulia, 2013)

$$\sigma = f_y + Q_\infty (1 - e^{-b\varepsilon_{pl}}) \quad (12)$$

Q∞ is the greatest change in the size of the yield surface and b is the rate at which the size of the yield surface varies as plastic strain develops, where f_y and ε_{pl} are the yield stress and plastic strain ($\varepsilon_{pl} = \varepsilon - \sigma/E$) of the steel, respectively. Both parameters of C_1 and γ_1 of Chaboche's model need to be validated with regard to the kinematic hardening section of the steel constitutive law.

The kinematic hardening part of the steel constitutive law reads (D. S. Simulia, 2013)

$$\alpha = \frac{c}{\gamma}(1 - e^{-\gamma\varepsilon_{pl}}) \quad (13)$$

2.2 Elements type and meshing size of the FE models

The model consisted of two parts: Concrete and steel tube. Concrete was modeled using the solid 8-node element C3D8R while steel tube was modeled using the shell 4 node element S4R. In the experimental test, reinforcing stiffening ribs were installed in the base along the direction of load, which can increase the foundation's stiffness and help it conform to the rigid body assumption. Consequently, the foundation was constructed as a rigid plate in the FE model for ease and quick simulation. The mesh size was chosen based on the mesh sensitivity analysis in the previous study (Osama & Sakr, 2023).

In the meanwhile, the model had a rigid plate installed on the column's top. The foundation and rigid plate were made with 4-node bilinear rigid quadrilateral R3D4 elements. To imitate the contact between the top and bottom rigid plates and the steel tube column, the tie function was used. An appropriate mesh type that ensured accurate results and quick calculation was targeted. The ideal element size was determined to be 5t for the steel and 10t for the concrete, where t is the tube thickness as shown in Fig. 3, and where the ideal element size is in the lateral and longitudinal directions. In Fig. 3, the standard FE model is displayed.

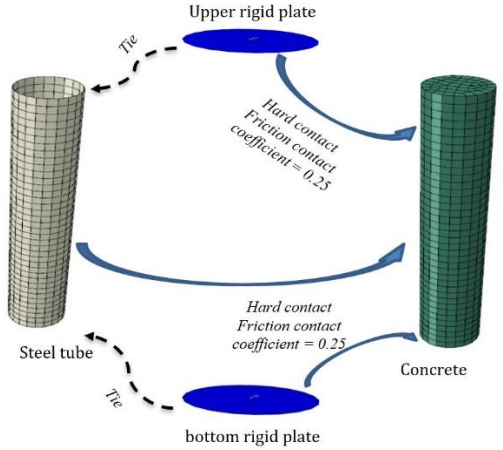

Fig. 3 The typical FEM

2.3 Contact interaction modeling

Surface-to-surface contact was utilized to simulate the interaction between the steel tube and the concrete, with "hard contact" being the criterion for normal behavior. The interface forces in tangential directions were created in accordance with the Coulomb friction model (Theofanous, Chan, & Gardner, 2009) in order to simulate the bond-slip effects between the concrete core and steel tube, where the constant friction coefficient was used as 0.25 (Yuan, Huang, & Chen, 2019).

3. Numerical results and discussion

In section 2 the material modeling were generally described then in this section these models will applied on the experimental study.

3.1 General descriptions of specimens

Previous work experimental data was utilized to validate the FEM models precision and applicability of NCFST and SFRRCFST columns under combined cyclic lateral loading and monotonic column axial load.

Experimental results of (Zhao et al., 2022) on 14 cantilever columns with 168 mm circular cross sections were published in their study the scale of the tested columns is 1/3 scale, and part of the specimens were chosen to validate the FEM. To look into the seismic performance of CFST columns with various parameters, including strength of concrete, axial load ratio, diameter-thickness ratio, and steel fiber ratio, specimens were designed and tested. Table 1 summarizes the characteristics and geometry of the experimentally tested specimens. (Zhao et al., 2022) presented the mixture design. As shown in Fig. 4, each of the specimens had a test length L of 950 mm, and this was measured from the lateral loading position to the highest point of the base stub.

Figure 4 demonstrates experimental set-up and loading system and how a fixed restriction that met the test criteria was created at the specimen's base. In the experimental set-up, the cap for the column was used with the following goals in mind: 1) When exposed to axial compression and lateral force, the specimen will not experience local compression failure or visible deformation if the top of the specimen is rigid. 2) Additionally, the actuator will be clamped to apply a horizontal load cling to the specimen.

Table 1. Characteristics and geometry of the experimentally tested specimens

Specimen	D (mm)	T (mm)	D/t	V_f (%)	f'_c (MPa)	f_y (MPa)	n	N (kN)
CRC-S	168	2.82	59.6	0	29.5	359.4	0.25	260.5
S1	168	2.82	59.6	1.2	32.1	359.4	0.25	271.9
S2	168	2.82	59.5	1.2	32.1	359.4	0.35	380.6
S3	168	2.82	59.6	1.2	32.1	359.4	0.45	489.4
S7	168	2.82	59.6	1.8	33.6	359.4	0.25	278.5
S8	168	3.70	45.4	1.2	32.1	375	0.25	316.4
S9	168	4.52	36.7	1.2	32.1	369.8	0.25	349.2

Note: The outer diameter(D), thickness of steel tube(t), volume ratio of steel fiber (V_f), cylinder compression strength of concrete (f'_c), yield strength of steel tube (f_y), axial compression ratio(n), Applied axial load (N).

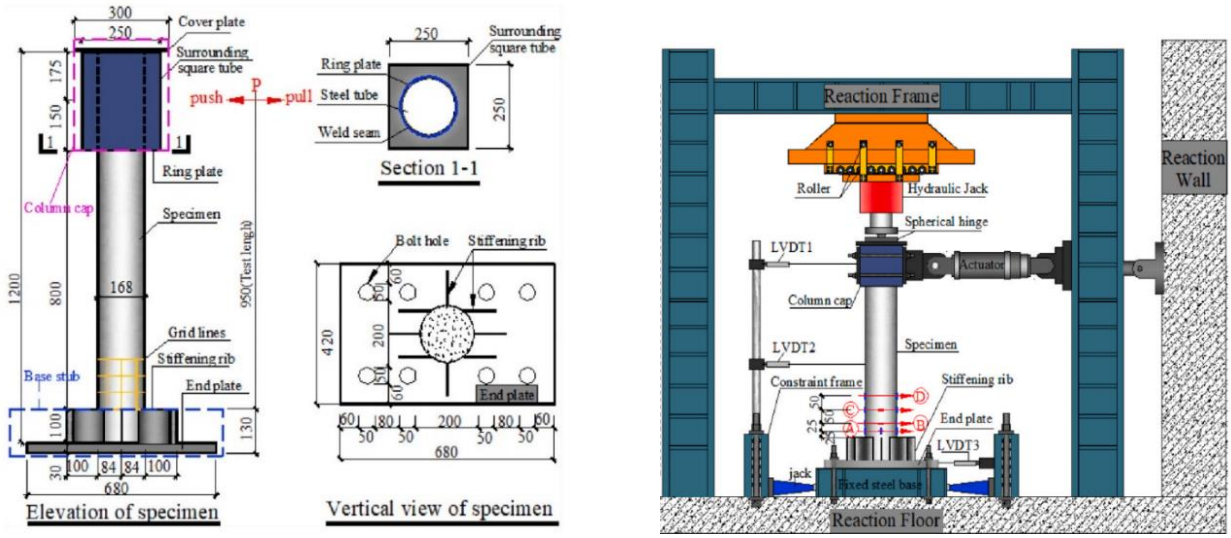

(a) (b)

Fig. 4 (a) The specimen diagram and (b) Experimental set-up and loading system (Zhao et al., 2022)

3.2 Material properties in the FEM

The NC and SFRRC nonlinear behavior can obviously be shown into two parts of the curves: tension and compression.

For instance, to f'_c=32.1MPa, the suggested constitutive model of confined concrete material under compression determined according to Eqs. (1)-(7), as shown in Fig. 5(a), and the elastic modulus of concrete according to Eqs. (6), E_c =26.6GPa.

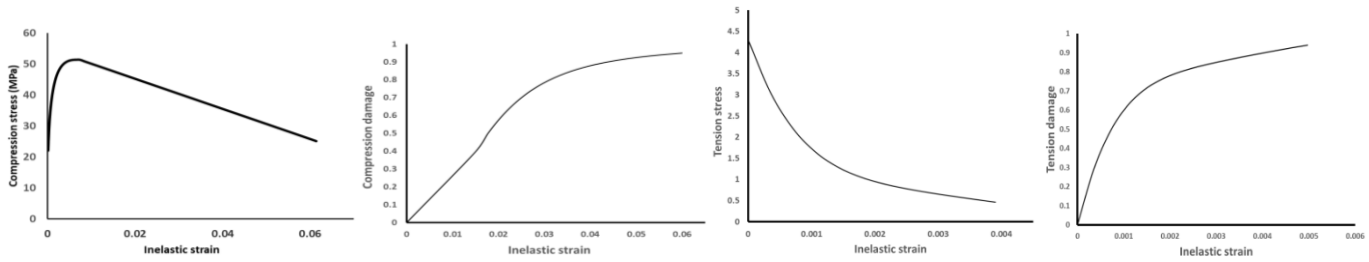

(a) (b) (c) (d)

Fig. 5 Concrete material properties (a) Compression stress-strain, (b) Concrete compression damage, (c) Tension Stress -strain and (d) Concrete tension damage

Table 2. Steel grades properties

Steel type	T [mm]	Es [GPa]	f_y [MPa]	f_u [MPa]	ν_s	Q_∞ [MPa]	b	C_1 [MPa]	γ_1
Qt3	2.82	210	359.4	461.5	0.27	21	1.2	7993	175
Qt4	3.70	208	375.0	469.6	0.26	21.9	1.25	8339	182
Qt5	4.52	205	369.8	369.8	0.26	21.6	1.23	8224	180

Fig.5(b). shows the compressive damage (d_c) has been calculated according to Eq. (8). The tension behavior was calculated according to Eq. (10) and tension damage(dt) according to Eq. (9), as shown in Fig.5 (c and d).

On measuring steel grades experimentally (Zhao et al., 2022) in terms of mechanical properties, these steel grades are illustrated in Table 2, namely, (i) yield strength (f_y) (ii) tensile strength (f_u) and (iii) elongation% (ε_u), while Table 2 shows the steel parameters under cyclic loading can be obtained by data fitting (Sakr et al., 2021; Wang, Shi, Wang, & Shi, 2013).

3.3 Loading and boundary conditions

The experimental specimens were tested under combined cyclic loading and axial compression. The axial compression was applied in the model as a uniform pressure (Fig. 6). During the cyclic protocol simulation, this axial load was kept constant. In order to apply the cyclic lateral loading, nodal horizontal displacements (dh) that were specified at the center of the above rigid steel plate were applied. The type of loading scheme applied in the lateral-loading was a displacement-controlled loading protocol (Zhao et al., 2022), as seen in Fig. 7. As indicated in Fig. 6, a boundary condition is determined at the bottom reference point aiming at the prevention of displacements and rotations totally. U2=0 and UR3=0 are the higher reference points.

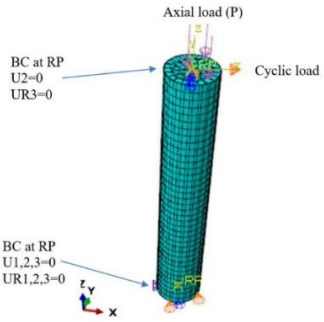

Fig. 6 Modeling of CFST columns

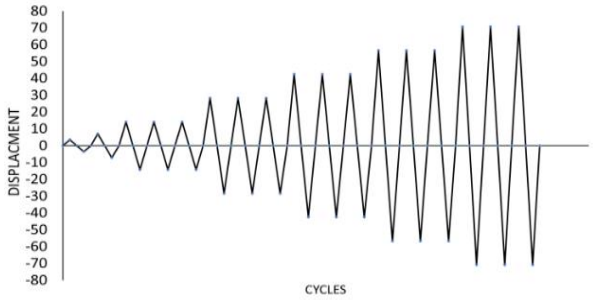

Fig. 7 Lateral load Protocol (Zhao et al., 2022)

Verification of the FEM

Effect of concrete confining pressure

The CDP model is used to analyze specimen S9 (Table 1) without considering the confining pressure from Eq. (3). As illustrated in Fig.8, FEM relationships of lateral load versus lateral displacement are compared with and without considering confined concrete and experimental result. The effect of using confined concrete has a little response on the computational cost of the model where the run time greater than the unconfined concrete by less than 5%.

Fig. 8 also shows that the CDP model is unable to make an accurate prediction of ultimate lateral load and lateral-strain behavior in the post-peak range without taking the confining pressure into account. To apply the CDP model in ABAQUS, the concrete confining pressure specified in Eq. (3) must be utilized.

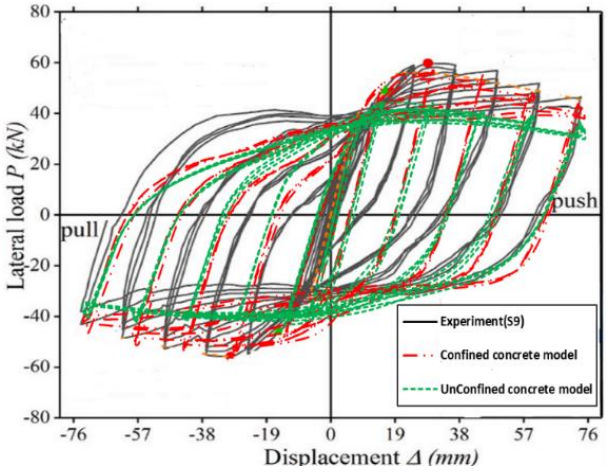

Fig. 8 Concrete confinement effect on lateral load-displacement hysteretic curves.

Comparison of experimental and finite element results

In this sub-section, Fig. 9 compares failure modes of both the experimental specimen and FEM. The columns plastic strains distributions are exhibited in figs. (9 and 10). A similar failure mode of compression bending was experienced remarkably in all the specimens. The concrete core and the steel tube bulged in both the compressive and tensile zones at the bottom, in addition to the existence of a crush of the concrete core, as can be observed in Figs. 9 and 10. This failure pattern of FEM was the same as that in the experiment. Figs. (9 and 10) illustrate the failure mode comparison between the experimental specimen and the FEM.

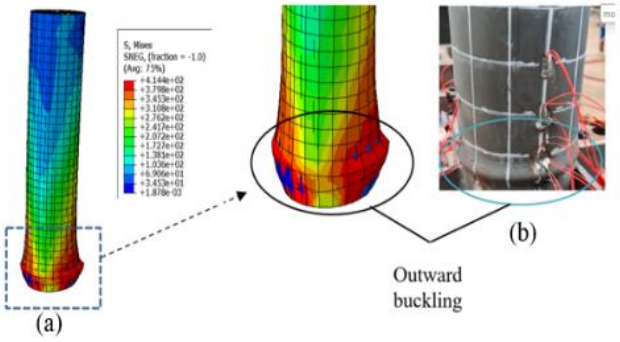

Fig. 9 Comparison of steel tube failure modes (a) FE modeling (steel tube plastic strain distribution at peak lateral load) and (b) Experimental

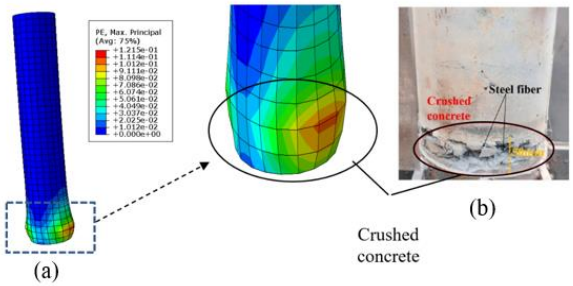

Fig. 10. Comparison of concrete failure modes (a) FE modeling (plastic strain distribution at peak lateral load) and (b) Experimental

Figures 11(a-g) illustrate the simulated outcomes of the non-linear analyses of the column models that were exposed to cyclic bending together with axial compression, comparing the experimental findings (Zhao et al., 2022). There is a trivial difference between simulated findings and experimental results, as seen in Figs.11(a-g). However, good agreement with each other was generally shown. Table 3 provides an overview of the experimental as well as simulated ultimate lateral load. The average of the mean values on dividing the ultimate lateral load of the finite element model by the experimental ultimate lateral loads was 0.936.

In conclusion, there was good observed compatibility between the experimental and simulation results. The FE models' precision and reliability were proven.

Table 3. Comparison between experimental ultimate lateral load and FE model results

Specimen label	P_{me} (kN)	P_{mf} (kN)	P_{mf}/P_{me}
CRC-S	39.4	37.3	0.946
S1	42.92	38.5	0.897
S2	42.79	39.3	0.918
S3	38.32	37.1	0.968
S7	43.28	39.1	0.903
S8	52.24	49.2	0.941
S9	57.73	56.5	0.978
Average values	-	-	0.936

Note: Ultimate Experimental lateral load (P_{me}), ultimate FE model lateral load (P_{mf}).

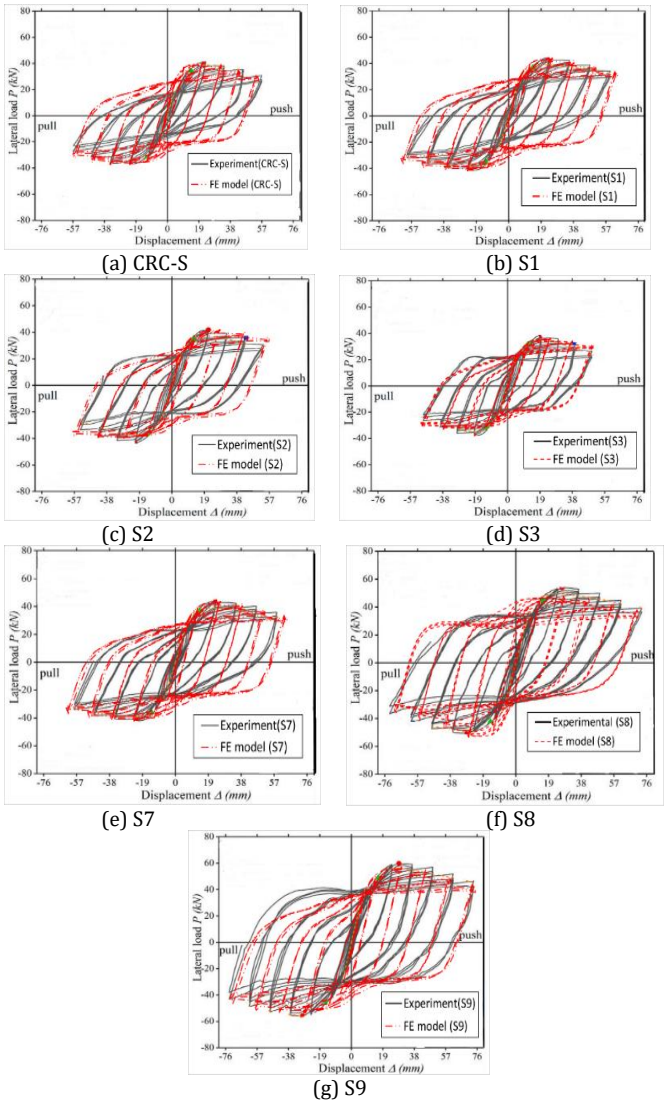

Fig. 11 Comparison of experimental and FE model hysteretic curves

In the first stage of loading, the behavior of the specimens appeared to be essentially elastic, as the curves appeared to almost overlap and had no major deformations, the energy dissipation appeared to be minimal. Then, the specimens gradually entered the plastic-elastic state. Moreover, the slope of the hysteretic loop began to decrease, which means that the lateral stiffness began to decrease. The specimens appeared to have a great ability to dissipate energy, as the hysterical loops were pumped. As the level of lateral displacement increased, residual lateral deformations clearly appeared. For each hysteretic loop, the lateral load continues to increase

until it reaches the maximum load. After that, a decrease in the lateral load appears, accompanied by a slight decrease in the descending branch, which indicates the good ductility of the element. The behavior of the specimens was greatly affected by changing the thickness of the tube and the axial pressure. As the thickness and axial pressure increased, the shape of the hysteretic curves became fuller. This indicates a significant improvement in energy dissipation at the same Iranian displacement. In general, all samples showed a continuous decrease in the secant stiffness as the loading stages progressed and lateral displacement increased. This may be due to increased lateral displacement, which causes accumulated damage. In the initial stages, the curves decrease rapidly, and then in the final stage they tend to flatten.

4. Conclusions

In this study, ABAQUS was used to conduct a numerical analysis of the cyclic behavior of normal and steel fiber reinforced recycled concrete-filled steel tubes (NCFST, SFRRCFST) columns with circular cross-section. This was performed under a combination of cyclic loading and monotonic column axial load. The numerical outcomes were contrasted with the experimental findings produced by (Zhao et al., 2022)after the numerical models had initially been described. The model novelty lies in the confinement behavior of NC and SFRRC in the FE model.

This study draws these main conclusions:

1. A precise prediction of the ultimate lateral loads, initial stiffness and stiffness degradation can be reached through the FEM developed for the NCFST and SFRRCFST columns and the average of the mean values on dividing the ultimate lateral load of the finite element model by the experimental ultimate lateral loads was 0.936.
2. Similarity in behaviors was obviously shown through the numerical and experimental hysteretic curves and failure modes. This indicates that the currently suggested FEM provides an accurate tool for representing the performance of NCFST and SFRRCFST columns.
3. On comparing lateral load versus story drift relationships of FEM with and without considering confined concrete and experimental result, it is clear that the (CDP) model cannot make an accurate prediction of the ultimate lateral load as well as lateral-strain behavior in the post-peak region without taking the confining pressure of concrete core into account. As a result, the CDP model in ABAQUS should employ concrete confining pressure.

References

ACI, A. (2014). Building code requirements for structural concrete and commentary. ACI 318, 14.

ACI Committee. (2008). Building code requirements for structural concrete (ACI 318-08) and commentary.

Aksoylu, C., Özkılıç, Y. O., Hadzima-Nyarko, M., Işık, E., & Arslan, M. H. (2022). Investigation on improvement in shear performance of reinforced-concrete beams produced with recycled steel wires from waste tires. Sustainability, 14(20), 13360.

Amin, M., Agwa, I. S., Mashaan, N., Mahmood, S., & Abd-Elrahman, M. H. (2023). Investigation of the physical mechanical properties and durability of sustainable ultra-high-performance concrete with recycled waste glass. Sustainability, 15(4), 3085.

Chaboche, J.-L. (1986). Time-independent constitutive theories for cyclic plasticity. International Journal of plasticity, 2(2), 149-188. https://doi:10.1016/0749-6419(86)90010-0

Chaboche, J.-L. (1989). Constitutive equations for cyclic plasticity and cyclic viscoplasticity. International Journal of plasticity, 5(3), 247-302. https://doi:10.1016/0749-6419(89)90015-6

Chang, X., Fu, L., Zhao, H.-B., & Zhang, Y.-B. (2013). Behaviors of axially loaded circular concrete-filled steel tube (CFT) stub columns with notch in steel tubes. Thin-Walled Structures, 73, 273-280. https://doi:10.1016/j.tws.2013.08.018

Chang, Y., Chen, W., Xiao, Q., Rong, E., & Peng, L. (2021). Theoretical and experimental study on axial compression concrete-filled tubes with different confinements. Journal of constructional steel research, 185, 106862. https://doi:10.1016/j.jcsr.2021.106862

Chen, J., Wang, J., Xie, F., & Jin, W.-l. (2016). Behavior of thin-walled dodecagonal section double skin concrete-filled steel tubes under bending. Thin-Walled Structures, 98, 293-300. https://doi:10.1016/j.tws.2015.10.002

Choi, C. S., Jung, H. S., & Choi, H. K. (2013). The behavior of concrete filled steel square-tube stub column with steel-fiber reinforced high strength concrete. Advanced Materials Research, 663, 125-129. https://doi:10.4028/www.scientific.net/AMR.663.125

Desayi, P., & Krishnan, S. (1964). Equation for the stress-strain curve of concrete. Paper presented at the Journal Proceedings.

Di, J., Fan, J., Zhou, X., Zhao, L., Han, B., Qin, F., & Zhang, Z. (2022). The hysteretic behavior of composite bridge columns with plastic hinge enhanced by engineered cementitious composite jacket for seismic resistance. Engineering Structures, 251, 113532. https://doi:10.1016/j.engstruct.2021.113532

Di, J., Han, B., Zhou, X., Hu, L., Qi, Y., & Qin, F. (2022). Experimental investigation into cyclic working performances of prefabricated CFST columns with improved column-footing connections. Journal of Building Engineering, 46, 103772. https://doi:10.1016/j.jobe.2021.103772

ELWakkad, N. Y., Heiza, K. M., & Mansour, W. (2023). Experimental study and finite element modelling of the torsional behavior of self-compacting reinforced concrete (SCRC) beams strengthened by GFRP. Case Studies in Construction Materials, 18, e02123.

Emad, W., Mohammed, A. S., Kurda, R., Ghafor, K., Cavaleri, L., Qaidi, S. M., . . . Asteris, P. G. (2022). Prediction of concrete materials compressive strength using surrogate models. Paper presented at the Structures.

Européen, C. (2004). Eurocode 2: Design of concrete structures—part 1-1: General rules and rules for buildings. London: British Standard Institution.

Fam, A., Qie, F. S., & Rizkalla, S. (2004). Concrete-filled steel tubes subjected to axial compression and lateral cyclic loads. Journal of structural engineering, 130(4), 631-640. https://doi:10.1061/(ASCE)0733-9445(2004)130:4(631)

Fantilli, A. P., Vallini, P., & Chiaia, B. (2011). Ductility of fiber-reinforced self-consolidating concrete under multi-axial compression. Cement and Concrete Composites, 33(4), 520-527. https://doi:10.1016/j.cemconcomp.2011.02.007

Fayed, S., Badr el-din, A., Basha, A., & Mansour, W. (2022). The shear behavior of RC pile cap beams strengthened using ultra high- performance concrete reinforced with steel mesh fabric. Case Studies in Construction Materials, 17, e01532.

Fayed, S., Madenci, E., Bahrami, A., Özkiliç, Y. O., & Mansour, W. (2023). Experimental study on using recycled polyethylene terephthalate and steel fibers for improving behavior of RC columns. Case Studies in Construction Materials, 19, e02344.

Fayed, S., Madenci, E., Özkiliç, Y. O., & Mansour, W. (2023). Improving bond performance of ribbed steel bars embedded in recycled aggregate concrete using steel mesh fabric confinement. Construction and Building Materials, 369, 130452.

Fayed, S., Madenci, E., Özkiliç, Y. O., & Tawfik, T. A. (2024). Effect of Block Size on Bearing Strength of Steel Fiber-Reinforced Recycled Aggregate Concrete. Arabian Journal for Science and Engineering, 49(4), 5287-5303.

Ge, H., & Usami, T. (1996). Cyclic tests of concrete-filled steel box columns. Journal of structural engineering, 122(10), 1169-1177. https://doi:10.1061/(ASCE)0733-9445(1996)122:10(1169)

Gopal, S. R., & Manoharan, P. D. (2006). Experimental behaviour of eccentrically loaded slender circular hollow steel columns in-filled with fibre reinforced concrete. Journal of constructional steel research, 62(5), 513-520. https://doi:10.1016/j.jcsr.2005.09.004

Hajjar, J. F., & Gourley, B. C. (1997). A cyclic nonlinear model for concrete-filled tubes. I: Formulation. Journal of structural engineering, 123(6), 736-744. https://doi:10.1061/(ASCE)0733-9445(1997)123:6(736)

Han, L.-H., Huang, H., Tao, Z., & Zhao, X.-L. (2006). Concrete-filled double skin steel tubular (CFDST) beam–columns subjected to cyclic bending. Engineering Structures, 28(12), 1698-1714. https://doi:10.1016/j.engstruct.2006.03.004

Han, L.-H., Li, W., & Bjorhovde, R. (2014). Developments and advanced applications of concrete-filled steel tubular (CFST) structures: Members. Journal of constructional steel research, 100, 211-228. https://doi:10.1016/j.jcsr.2014.04.016

Hognestad, E. (1951). Study of combined bending and axial load in reinforced concrete members. University of Illinois. Engineering Experiment Station. Bulletin; no. 399.

Hu, H.-T., Huang, C.-S., Wu, M.-H., & Wu, Y.-M. (2003). Nonlinear analysis of axially loaded concrete-filled tube columns with confinement effect. Journal of structural engineering, 129(10), 1322-1329. https://doi:10.1061/(ASCE)0733-9445(2003)129:10(1322)

Ibañez, C., Hernández-Figueirido, D., & Piquer, A. (2021). Effect of steel tube thickness on the behaviour of CFST columns: Experimental tests and design assessment. Engineering Structures, 230, 111687. https://doi:10.1016/j.engstruct.2020.111687

Jaf, D. K. I., Abdulrahman, P. I., Mohammed, A. S., Kurda, R., Qaidi, S. M., & Asteris, P. G. (2023). Machine learning techniques and multi-scale models to evaluate the impact of silicon dioxide (SiO2) and calcium oxide (CaO) in fly ash on the compressive strength of green concrete. Construction and Building Materials, 400, 132604.

Kent, D. C., & Park, R. (1971). Flexural members with confined concrete. Journal of the structural division, 97(7), 1969-1990. https://doi:10.1061/JSDEAG.0002957

Lai, M. H., & Ho, J. (2015). Axial strengthening of thin-walled concrete-filled-steel-tube columns by circular steel jackets. Thin-Walled Structures, 97, 11-21. https://doi:10.1016/j.tws.2015.09.002

Liang, Q. Q. (2009). Performance-based analysis of concrete-filled steel tubular beam–columns, Part I: Theory and algorithms. Journal of constructional steel research, 65(2), 363-372. https://doi:10.1016/j.jcsr.2008.03.007

Liu, J., Zhou, X., & Zhang, S. (2008). Seismic behaviour of square CFT beam–columns under biaxial bending moment. Journal of constructional steel research, 64(12), 1473-1482. https://doi:10.1016/j.jcsr.2008.01.013

Liu, X., Liu, J., Yang, Y., Cheng, G., & Lanning, J. (2020). Resistance of special-shaped concrete-filled steel tube columns under compression and bending. Journal of constructional steel research, 169, 106038. https://doi:10.1016/j.jcsr.2020.106038

Liu, Z., Lu, Y., Li, S., & Liao, J. (2019). Axial behavior of slender steel tube filled with steel-fiber-reinforced recycled aggregate concrete. Journal of constructional steel research, 162, 105748.

Liu, Z., Lu, Y., Li, S., & Liao, J. (2021). Shear response of steel fiber reinforced recycled concrete-filled steel tube columns. Advances in Structural Engineering, 24(12), 2684-2704.

Liu, Z., Lu, Y., Li, S., Zong, S., & Yi, S. (2020). Flexural behavior of steel fiber reinforced self-stressing recycled aggregate concrete-filled steel tube. Journal of cleaner production, 274, 122724.

Lu, Y.-y., Li, N., Li, S., & Liang, H.-j. (2015). Experimental investigation of axially loaded steel fiber reinforced high strength concrete-filled steel tube columns. Journal of Central South University, 22(6), 2287-2296. https://doi:10.1007/s11771-015-2753-x

Lu, Y., Li, N., Li, S., & Liang, H. (2015). Behavior of steel fiber reinforced concrete-filled steel tube columns under axial compression. Construction and Building Materials, 95, 74-85. https://doi:10.1016/j.conbuildmat.2015.07.114

Lue, D. M., Liu, J.-L., & Yen, T. (2007). Experimental study on rectangular CFT columns with high-strength concrete. Journal of constructional steel research, 63(1), 37-44. https://doi:10.1016/j.jcsr.2006.03.007

Madenci, E., Fayed, S., Mansour, W., & Özkılıç, Y. O. (2022). Buckling performance of pultruded glass fiber reinforced polymer profiles infilled with waste steel fiber reinforced concrete under axial compression. Steel and Composite Structures, An International Journal, 45(5), 653-663.

Mander, J. B., Priestley, M. J., & Park, R. (1988). Theoretical stress-strain model for confined concrete. Journal of structural engineering, 114(8), 1804-1826. https://doi:10.1061/(ASCE)0733-9445(1988)114:8(1804)

Mansour, W., Li, W., Wang, P., & Badawi, M. (2024). Experimental and numerical evaluations of the shear performance of recycled aggregate RC beams strengthened using CFRP sheets. Engineering Structures, 301, 117368.

Morishita, Y. (1982). Experimental Studies on Bond Strength between Square Steel Tube in Concrete Filled and Encased Concrete Core under Cyclic Shearing Force and Constant Axial Force. Transactions of the Japan Concrete Institute, 4, 363-370. https://doi:10.1016/j.tws.2021.108506

Nguyen, T.-T., Thai, H.-T., Ngo, T., Uy, B., & Li, D. (2021). Behaviour and design of high strength CFST columns with slender sections. Journal of constructional steel research, 182, 106645. https://doi:10.1016/j.jcsr.2021.106645

Osama, B., & Sakr, M. (2023). Modeling of Ultra-high Performance Fiber Reinforced Concrete Filled Steel Tube Columns under Eccentric Loading. Periodica Polytechnica Civil Engineering, 67(1), 10-23. https://doi:10.3311/PPci.20593

Probst, A. D., Kang, T. H.-K., Ramseyer, C., & Kim, U. (2010). Composite flexural behavior of full-scale concrete-filled tubes without axial loads. Journal of structural engineering, 136(11), 1401-1412. https://doi:10.1061/(ASCE)ST.1943-541X.0000241

Qu, X., Xie, Y., Sun, G., Liu, Q., & Wang, H. (2023). Seismic Behavior of Assembly Joint with CFST Column and H-shaped Steel Beam. KSCE Journal of Civil Engineering, 27(2), 670-683. https://doi:10.1007/s12205-022-0781-2

Richart, F. E., Brandtzæg, A., & Brown, R. L. (1928). A study of the failure of concrete under combined compressive stresses. University of Illinois. Engineering Experiment Station. Bulletin; no. 185.

Saad, A. G., Sakr, M. A., Khalifa, T. M., & Darwish, E. A. (2023). Numerical analysis of rubberized engineered cementitious composite (RECC) RC beams under impact loads. Construction and Building Materials, 409, 134162.

Sakr, M. A., El-Khoriby, S. R., Seleemah, A. A., Aboelnour, M. M., & Osama, B. (2021). Experimental and numerical investigation on cyclic behavior of masonry infilled RC frames retrofitted with partially bonded CFRP strips. Structures, 33, 2238-2252. https://doi:10.1016/j.istruc.2021.05.087

Sakr, M. A., Saad, A. G., & El-korany, T. M. (2022). Analysis of exterior beam-column joints under varying column axial load and code comparisons. Advances in Structural Engineering, 25(4), 837-863. https://doi:10.1177/13694332211050979

Simulia, A. U. M. (2007). Abaqus Version 6.7. 1. Dassault Systémes.

Simulia, D. S. (2013). ABAQUS 6.13 User's manual. Dassault Systems, Providence, RI, 305, 306.

Song, P., & Hwang, S. (2004). Mechanical properties of high-strength steel fiber-reinforced concrete. Construction and Building Materials, 18(9), 669-673. https://doi:10.1016/j.conbuildmat.2004.04.027

Tam, L.-h., Minkeng, M. A. N., Lau, D., Mansour, W., & Wu, C. (2023). Molecular interfacial shearing creep behavior of carbon fiber/epoxy matrix interface under moisture condition. Engineering Fracture Mechanics, 282, 109177.

Tao, Z., Wang, Z.-B., & Yu, Q. (2013). Finite element modelling of concrete-filled steel stub columns under axial compression. Journal of constructional steel research, 89, 121-131. https://doi:10.1016/j.jcsr.2013.07.001

Theofanous, M., Chan, T. M., & Gardner, L. (2009). Structural response of stainless-steel oval hollow section compression members. Engineering Structures, 31(4), 922-934. https://doi:10.1016/j.engstruct.2008.12.002

Tokgoz, S., & Dundar, C. (2010). Experimental study on steel tubular columns in-filled with plain and steel fiber reinforced concrete. Thin-Walled Structures, 48(6), 414-422. https://doi:10.1016/j.tws.2010.01.009

Tu, C., Shi, Y., Liu, D., Wang, W., & Ban, H. (2021). Behavior and general design method of concrete-filled high-strength steel tube (CFHST) columns. Engineering Structures, 243, 112506. https://doi:10.1016/j.engstruct.2021.112506

Wang, M., Shi, Y., Wang, Y., & Shi, G. (2013). Numerical study on seismic behaviors of steel frame end-plate connections. Journal of constructional steel research, 90, 140-152. https://doi:10.1016/j.jcsr.2013.07.033

Xiao, J., & Xiao, J. (2018). Recycled aggregate concrete: Springer.

Xu, S., Wu, C., Liu, Z., & Shao, R. (2019). Experimental investigation on the cyclic behaviors of ultra-high-performance steel fiber reinforced concrete filled thin-walled steel tubular columns. Thin-Walled Structures, 140, 1-20. https://doi:10.1016/j.tws.2019.03.008

Yıldızel, S. A., Özkılıç, Y. O., Bahrami, A., Aksoylu, C., Başaran, B., Hakamy, A., & Arslan, M. H. (2023). Experimental investigation and analytical prediction of flexural behaviour of reinforced concrete beams with steel fibres extracted from waste tyres. Case Studies in Construction Materials, 19, e02227.

Yildizel, S. A., Özkılıç, Y. O., & Yavuz, A. (2024). Optimization of waste tyre steel fiber and rubber added foam concretes using Taguchi method and artificial neural networks. Paper presented at the Structures.

Yu, X. Q., Lin, M., Geng, G. L., Wei, N., & Jia, L. (2013). Study on mechanical properties of steel fiber reinforced concrete. Applied Mechanics and Materials, 252, 280-284. https://doi:10.4028/www.scientific.net/AMM.252.280

Yuan, F., Huang, H., & Chen, M. (2019). Effect of stiffeners on the eccentric compression behaviour of square concrete-filled steel tubular columns. Thin-Walled Structures, 135, 196-209. https://doi:10.1016/j.tws.2018.11.015

Zeybek, Ö., Özkılıç, Y. O., Çelik, A. İ., Deifalla, A. F., Ahmad, M., & Sabri Sabri, M. M. (2022). Performance evaluation of fiber-reinforced concrete produced with steel fibers extracted from waste tire. Frontiers in Materials, 9, 1057128.

Zhao, P., Huang, Y., Liu, Z., Wang, H., & Lu, Y. (2022). Experimental research on seismic performance of steel fiber-reinforced recycled concrete-filled circular steel tube columns. Journal of Building Engineering, 54, 104683. https://doi: 10.1016/j.jobe.2022.104683

Zhu, A., Zhang, X., Zhu, H., Zhu, J., & Lu, Y. (2017). Experimental study of concrete filled cold-formed steel tubular stub columns. Journal of constructional steel research, 134, 17-27. https://doi:10.1016/j.jcsr.2017.03.003

Zhu, H., Zhang, H., & Liu, L. (2021). Experimental Study on Cyclic Lateral Loaded Circular CFST Members with Initial Imperfections. KSCE Journal of Civil Engineering, 25(8), 3064-3074. https://doi:10.1007/s12205-021-1931-7